



Contents lists available at ScienceDirect

Methods

journal homepage: [www.elsevier.com/locate/ymeth](http://www.elsevier.com/locate/ymeth)

Review Article

## PALM and STORM: Into large fields and high-throughput microscopy with sCMOS detectors

Pedro Almada, Siân Culley, Ricardo Henriques\*

Quantitative Imaging and NanoBiophysics Group, MRC Laboratory for Molecular Cell Biology and Department of Cell and Developmental Biology, University College London, Gower Street, WC1E 6BT London, United Kingdom

## ARTICLE INFO

## Article history:

Received 11 March 2015  
 Received in revised form 28 May 2015  
 Accepted 3 June 2015  
 Available online xxxx

## Keywords:

Single-molecule localization  
 Hardware  
 sCMOS  
 Homogenization

## ABSTRACT

Single Molecule Localization Microscopy (SMLM) techniques such as Photo-Activation Localization Microscopy (PALM) and Stochastic Optical Reconstruction Microscopy (STORM) enable fluorescence microscopy super-resolution: the overcoming of the resolution barrier imposed by the diffraction of light. These techniques are based on acquiring hundreds or thousands of images of single molecules, locating them and reconstructing a higher-resolution image from the high-precision localizations. These methods generally imply a considerable trade-off between imaging speed and resolution, limiting their applicability to high-throughput workflows. Recent advancements in scientific Complementary Metal-Oxide Semiconductor (sCMOS) camera sensors and localization algorithms reduce the temporal requirements for SMLM, pushing it toward high-throughput microscopy. Here we outline the decisions researchers face when considering how to adapt hardware on a new system for sCMOS sensors with high-throughput in mind.

© 2015 Elsevier Inc. All rights reserved.

### 1. Introduction to super-resolution microscopy

In past decades, the use of fluorescence microscopy has allowed modern cell biology labs to achieve considerable milestones in our knowledge of cell structure and organization [1]. However, information obtained from fluorescence microscopy has been limited by its resolution. A conventional optical microscope can only resolve structures down to approximately 300 nm, depending on numerical aperture and wavelength of light used. This is due to the diffraction of light as it passes through the microscope's optical elements [2,3]. For greater resolution, electron microscopy (EM) takes advantage of the <1 nm wavelength of electrons, resolving sub-nanometer features [4]. Many biological molecules, structures and processes exist on scales outside the resolution limit of conventional fluorescence microscopy. For example, microtubules have an outer diameter of 25 nm and a 12 nm inner diameter [5]; chromatin fibers have a width of 30 nm [6]; the prokaryotic ribosome has a diameter of c.a. 20 nm [7]. EM can resolve these

features but cannot accurately distinguish between molecular species, whereas fluorescence microscopy can selectively label a wide variety of biological molecules. Additionally, EM sample preparation is generally difficult, artifact prone, lengthy and strictly limited to fixed (dead) samples.

The field of super-resolution (SR) has emerged in recent years as a solution possessing the benefits of fluorescence microscopy but with resolution improved by an order of magnitude. Three major SR methods are now experiencing widespread adoption and commercial success: Stimulated Emission Depletion microscopy (STED) [8], Structured Illumination Microscopy (SIM) [9] and Single Molecule Localization Microscopy (SMLM) [10–12]. SMLM methods have relatively simple hardware requirements compared to STED or SIM. STED is based on a confocal laser scanning system with the requisite addition of a powerful second laser and specialized optics to generate a donut-shaped beam able to deplete fluorophore emission in the periphery of the illuminating spot, thus reducing the size of the emission spot and improving resolution [8]. SIM also requires specialized hardware to shape the excitation light such as motorized grids or spatial light modulators; this method radially increases the high-frequencies of the acquired images in a sequential manner and depends on computational processes to merge this information into a super-resolution image [13]. With SMLM however, the difference to a normal widefield microscope mostly falls on a careful choice of its hardware components and can be achieved on most commonly available widefield

*Abbreviations:* SR, super-resolution; SMLM, Single-Molecule Localization Microscopy; sCMOS, scientific Complementary Metal-Oxide Semiconductor; EMCCD, Electron-Multiplying Charge Coupled Device; SNR, signal-to-noise ratio; FOV, field of view; TIRF, Total Internal Reflection Fluorescence; FPS, frames per second; HILO, highly inclined and laminated optical sheet; BFP, Back Focal Plane; HT, high throughput; PSF, point spread function; ROI, Region of Interest.

\* Corresponding author.

E-mail address: [r.henriques@ucl.ac.uk](mailto:r.henriques@ucl.ac.uk) (R. Henriques).<http://dx.doi.org/10.1016/j.ymeth.2015.06.004>

1046-2023/© 2015 Elsevier Inc. All rights reserved.

microscopes with simple or no modifications [14]. For this reason it remains a highly attractive option for researchers considering SR methods. With recent developments in sCMOS camera technology and localization algorithms, SMLM can now reach speeds at full field of view (FOV) that are showing great promise for high-throughput (HT) imaging. But there are challenges in implementing this technology for researchers new to the field, as the literature assumes a certain practical body of knowledge. Here we walk the reader through their options and challenges when considering to adapt their imaging systems or assembling hardware to perform SMLM with a focus on large field of view, high throughput, high speed imaging utilizing sCMOS cameras. As throughput can also be increased by reducing the number of frames required for a single reconstruction, we also discuss recently developed SMLM algorithms capable of extracting meaningful results from fewer frames. In particular, we direct the reader to such algorithms with publicly available code.

### 1.1. Single Molecule Localization Microscopy (SMLM)

In a standard fluorescence microscope, the majority of excited fluorophores will emit light near-simultaneously. If they are separated by a distance smaller than the diffraction-limited resolution of the microscope, then they cannot be accurately distinguished from each other. But if they are at a distance greater than the resolution, they can be localized in an image with a precision which is greater than the diffraction limited spatial resolution of the microscope system; this precision generally scales with the square root of the number of photons collected from the fluorophore [15]. Most current SMLM methods are based on ensuring that only a small randomly changing subset of the fluorophores emits in each frame, thus allowing images to be captured where individually emitting fluorophores can be resolved. If only a sparse subset of molecules are emitting in each frame, it is likely most are separated from each other by a distance greater than the resolution limit. By imaging multiple different fractions of the fluorophore population over time a reconstructed image of the sample can be made from all the localizations which will reveal the entire structure.

Two major methods exist: Photoactivation Localization Microscopy (PALM [10,11]) and Stochastic Optical Reconstruction Microscopy (STORM [12,16]). The major distinctions between the two methods are the type of labels used, and how their fluorescence emission is modulated. PALM utilizes fluorophores whose emitting stage can be directly controlled such as photoactivatable proteins including PA-GFP, Dronpa and mEos2. A typical PALM imaging cycle will require activation of a small, random subset of fluorescent proteins by illumination with activating laser light. This subset of molecules is then imaged and subsequently bleached with a high power excitation laser, reducing their probability of appearing in further acquired frames. The cycle is then repeated starting with the activation of another random subset of proteins. This cycle is repeated many times until a sufficient number of localizations can be made in order to reconstruct the structure of interest [10,11].

STORM mostly uses fluorophores which stochastically turn their emission on and off, which is usually achieved with a combination of using organic dyes, such as Alexa- and Cy-dyes, and adequate buffer and illumination conditions [17]. These dyes are typically capable of emitting an order of magnitude more photons in a given time frame compared to the genetically encoded photoactivatable proteins used in PALM [16]. As discussed above, the lower number of photons collected in PALM will subsequently limit resolution [15]. The inherent photochemistry of fluorophores commonly used in STORM allows them to easily enter reversible long-lived dark states (tens of milliseconds, to several seconds, to

several hours in an oxygen-free environment) which allows their emission to be modulated [16,18–20]. These states are distinct from bleaching, which is an irreversible process. One of the simplest STORM methods, “direct STORM” (dSTORM) is based on inducing switching behavior by exciting the fluorophore in the presence of a buffer solution containing thiols (such as mercaptoethylamine (MEA) [21], beta-mercaptoethanol (BME), or recently TCEP [22]) and/or an oxygen scavenging system (ROXS [23]). Comprehensive evaluations of the various fluorophores and buffers used in dSTORM are available elsewhere [16,24]. Dyes can also be induced to re-enter an activated state through excitation with UV or near UV light such as that provided by a 405 nm laser commonly present on most microscopes [16].

The basic hardware requirements for SMLM are a widefield or Total Internal Reflection Fluorescence (TIRF) microscope, a sensitive camera and a sufficiently powerful illumination source, generally lasers (as opposed to lamps or Light Emitting Diodes (LEDs) commonly used in conventional widefield microscopy) [3]. In PALM two lasers are usually used: an activating laser and an excitation/bleaching laser, both of which must match the spectral properties of the fluorophore of interest. The overwhelming majority of photoactivatable fluorophores can be activated with UV or near UV laser light such as that from 405 nm lasers [25]. However, should the protein activate spontaneously, only an excitation laser is required as in the “PALM with independently running acquisition” (PALMIRA) method [26]. In dSTORM, although a UV or near UV laser can be used to reactivate the fluorophores, modulation of the photoswitching behavior can be achieved solely by adjusting the excitation laser power. This means that the only major hardware difference between PALM and STORM systems is the power of the lasers, as higher laser intensities are usually required in STORM than PALM [16].

### 1.2. Speed and throughput limitations of HT super-resolution microscopy

For HT microscopy, both reducing acquisition time and increasing FOV will increase the throughput. Any reduction of acquisition time or the need to repeat steps will considerably accelerate an HT project given that a typical workflow will require repeating the same actions hundreds, if not thousands of times. When designing an HT project that might require super-resolution, the choice of SR method has to take into account throughput, ease of sample preparation and instrument complexity.

Of the three major techniques (Table 1), SIM imposes the fewest requirements on sample preparation making it highly attractive for HT. Although SIM requires a high SNR in its acquired images to avoid artifacts in reconstructions, it remains the fastest SR technique and commercial instruments already make use of large FOV sCMOS cameras. However, SIM also remains the most resolution-limited technique, being capable of only a doubling of resolution with currently available instruments, limiting its

**Table 1**

Qualitative comparison of the three most common super-resolution methods. The resolutions mentioned refer to what is routinely achievable with biological samples; frame-rate compares best-case scenarios to acquire large FOV areas with the above mentioned resolutions; instrument complexity is an evaluation of how hard large FOV systems are to implement in modern labs, either manually or with commercial systems.

	SIM	STED	SMLM
Resolution (nm)	100	70–60	30–20
Frame-rate	10 hz	30 hz	0.1 hz
Instrument complexity	High	Very high	Low
Sample requirements	Very low	High	Medium

**Table 2**

Calculating expected total throughput after reducing the FOV by either cropping whole lines (l) or choosing square regions of interest (s). sCMOS technology only yields a speed increase for each cropped line, not columns so the speed increase from cropping square regions is the same as when reducing the corresponding number of lines. Fold area decrease (l) =  $2048^2/n_{\text{lines}} * 2048$ ; fold area decrease (s) =  $2048^2/n_{\text{lines}}^2$ ; throughput decrease (l) =  $(n_{\text{lines}} * 2048)/2048^2$ ; throughput decrease (s) =  $(n_{\text{lines}}^2)/2048^2$ ; speed increase = FPS/100; total throughput (TT) = throughput decrease \* speed increase.

$n_{\text{lines}}$	FPS	Fold area decrease (l)	Fold area decrease (s)	Throughput decrease (l)	Throughput decrease (s)	Speed increase	TT (l)	TT (S)
2048	100	1	1	1	1	1	1	1
1024	200	2	4	0.5	0.25	2	1	0.5
512	400	4	16	0.25	0.0625	4	1	0.25
256	800	8	64	0.125	0.015625	8	1	0.125
128	1600	16	256	0.0625	0.00390625	16	1	0.0625
64	3200	332	1024	0.03125	0.00097656	32	1	0.03125

applicability. STED has theoretically unlimited resolution but is slowed by the need to scan a spot over the area to be imaged; reducing this area increases the available speed at which SR images can be acquired. For example, Westphal et al. [27] achieved 28 frames per second imaging of synaptic vesicles at 60 nm resolution by restricting the FOV to a  $2.8 \times 1.5 \mu\text{m}$  region. One way to increase the speed of STED is to parallelize and scan several spots over a large area. Recently, Bergermann et al. [28] scanned 2500 spots over a  $20 \mu\text{m}$  diameter region resulting in STED images of vimentin with 68 nm resolution. Theoretically, the whole FOV of an objective can be imaged in this way. However, such parallelized systems are restricted to the few labs who can assemble them and furthermore, STED microscopy in general imposes considerable limitations on dye choice, is limited to 2 colors for multicolor imaging and most labs find it hard to improve the resolution to below 60 nm on biological samples.

Compared to SIM and STED, SMLM is considerably slower. Each reconstructed image requires thousands of frames to be acquired in order to collect enough photons for a sufficient number of fluorophore localizations (commonly millions to billions) to accurately represent cellular structures, since only a few molecules (generally hundreds) should be emitting in each frame. However, it requires less specialist hardware than STED or SIM, multicolor imaging is straightforward, and resolutions of 30 nm in biological samples can be achieved with some regularity, which makes it a more attractive technique for HT projects involving fine structural details. Indeed, SMLM has already been used in HT studies: Holden et al. [29] used HT PALM with 35 nm resolution to reveal the in vivo 3D organization of FtsZ in the bacterial Z ring. SMLM is also ideally suited for imaging signaling events, a common target for screens and HT projects. For example, Soares et al. [30] used HT dSTORM with 19 nm localization precisions to reveal signaling territories controlling T Cell activation.

The overwhelming majority of publicly available SMLM analysis software assumes that individual fluorophores do not spatiotemporally overlap extensively, and so the speed at which frames can be acquired depends on the amount of time a molecule spends on the emitting state. The shorter this 'emitting state' lasts, the faster the possible frame-rate is [16,31]. The lifetime of this state can be reduced by increasing the excitation laser intensity, or by using specialist buffers in the case of STORM [16]. The limiting step then becomes the read-out speed of the camera, one of the advantages of sCMOS cameras, and how many frames need to be acquired per reconstruction. While reducing the exposure time reduces the number of collected photons per molecule per frame, it also reduces the number of background photons collected, reducing the impact of low exposure times on resolution. This has been recently demonstrated and quantified by Lin et al. [32] for Alexa 647, which show speeds of 1600 FPS (for a cropped sCMOS FOV) can achieve resolutions comparable to slower acquisition speeds and reaching satisfactory localization densities in a matter of seconds. This resulted in a 16-fold reduction in acquisition time when compared to the full FOV speed at 100 FPS (Table 2). However, the

throughput was limited as, to achieve such speeds, the FOV had to be reduced to a square area 256 times smaller than the full FOV. Table 2 details the relationship between cropping the FOV of an sCMOS camera and its resultant throughput; from this it is evident that trading off area for speed does not increase throughput. In addition, each fold-decrease in area will require moving parts to cover an area equivalent to the whole FOV, slowing down an HT workflow. As such, using the whole FOV of the sCMOS is a more attractive proposition for HT SMLM.

More importantly, new algorithms have been and are currently under development that are capable of handling overlapping fluorophores, allowing for use of fluorophores with less favorable blinking statistics in high-speed SMLM (see Section 2.6.2), as well as reducing the total number of frames needed to acquire. The total time to acquire frames for a single reconstruction will depend on the density of recovered fluorophores and current algorithms require tens of thousands of fluorophores: even at 1600 FPS a 30,000 frame acquisition will take around 18 s, clearly slower than SIM or STED. One advantage for HT, however, is 3D SMLM. 3D methods for SMLM extract the extra dimension from data from a single focus position (see Section 2.3.1), which means extra information can be extracted at no cost to the acquisition time, something neither SIM nor STED are capable of.

Developments in sensor technology, dye chemistry, buffer conditions and algorithms should all lead to ever shorter acquisition times, making SMLM comparable to the speeds of SIM and STED but with enhanced resolution and simplified sample and instrument requirements. Below we will guide users on the considerations of assembling the hardware necessary to take advantage of sCMOS cameras for large FOV high-throughput SMLM.

## 2. Basis of assembling a high-throughput SMLM system

The main focus of the hardware considerations described in this review is designing a HT SMLM system which takes advantages of sCMOS cameras: namely their large field of view and short exposure times enabling higher throughput.

### 2.1. Excitation path

The localization precision of individual fluorophores is highly perturbed by the unwanted background intensity of the image, as differentiating between photons coming from the fluorophore to be localized and photons from other sources becomes more challenging [15]. The ratio between the true signal from the fluorophore of interest relative to the background photons and noise is generally defined as the signal-to-noise ratio (SNR). The higher the contribution from the background, the lower the SNR and therefore the precision. To reduce the contribution of unwanted background, most SMLM applications use Total Internal Reflection Fluorescence (TIRF), a technique that significantly constrains the excitation depth at the surface of a coverslip [33,34].

**Table 3**

Qualitative comparison of the performance of the three mentioned illumination methods; system complexity refers to complexity when implementing in custom systems; efficiency refers to power loss before the entering objective; sample penetration refers to how deep in the sample imaging can be performed; restrictions refers to whether the technique imposes restrictions on the usable refractive index of the sample medium and/or NA of the objective.

	TIRF	HILO	Widefield
System complexity	Moderate	Moderate	Low
Background reduction	Best	Good	None
Efficiency	Reasonable	Reasonable	Best
Sample penetration	<~100 nm	<~50 $\mu\text{m}$	<~100 $\mu\text{m}$
Restrictions	Media; NA	Media; NA	None

This is achieved through total internal reflection at the interface between two media with different refractive indices (i.e. the glass coverslip and the sample in aqueous media), where an evanescent wave is created whose intensity decays exponentially with distance from the interface. As a result, in TIRF microscopy there is selective excitation of molecules very close to the coverslip up to a depth of 60–100 nm [35], reducing out-of-focus fluorescence and enhancing the SNR [10,12,21]. For total internal reflection to occur, the excitation light must be incident on the interface at the ‘critical angle’ or higher [36]; this angle is defined by the difference between the refractive indices at the interface. The numerical aperture (NA) of the objective determines the maximum angle at which light can be incident on the sample, and as such TIRF typically requires an objective with an NA of 1.33 or higher [36]. In practice, TIRF objectives have higher NAs as these are capable of readily exceeding the critical angle. An added advantage is that high NA objectives collect more light and therefore provide better SNR at the same magnification [35]. Given that most commercially available TIRF systems automatically fulfill the criteria for PALM or STORM imaging (laser illumination, sensitive cameras, high NA objectives), these can be and are used for SMLM. A similar technique called highly inclined and laminated optical sheet (HILO) microscopy makes use of a highly inclined light beam to generate a thin optical sheet that penetrates the sample at a shallow angle. HILO has been used effectively in single-molecule fluorescence nanoscopy of the cell nucleus with high signal/background ratios [37]. Table 3 offers a qualitative comparison of using either wide-field illumination, TIRF or HILO.

Objective lenses for large FOV imaging should ideally have corrections for “flatness of field”, as uncorrected lenses will have significant aberrations and intensity variations between the center and the edges of the FOV. Objectives with such FOV corrections are labeled “Plan” and should have an intensity difference of no more than 20% between the center and the edge of the FOV [38]. However, high NA objectives used for TIRF, as discussed above, often do not correct for flatness of field as effectively as lower NA objectives. This results in TIRF being limited to a smaller FOV at the center which is actually in focus and has minimal chromatic and spherical aberrations; uncorrected areas will have severely reduced SNR [39]. While manufacturers may claim to have Plan corrected objectives with NA > 1.4, this correction may be only up to a quality standard that may vary between brands. Interested buyers should require the manufacturer to disclose the extent of the correction. Thus, while sCMOS cameras enable a much larger FOV to be acquired for high-throughput imaging, this will actually be limited by the objective corrections as the FOV may be restricted to the Plan corrected central region of the objective.

### 2.1.1. Laser launching

Since SMLM generally requires high illumination intensities, input of the laser beams into the microscope objective should be done with maximum possible efficiency. There are two immediate

choices: whether to use mirrors to launch the laser directly (in free space) to the microscope, or by launching through an optical fiber (Fig. 1). While launching directly minimizes optical light losses, fiber launching has a few advantages: it provides long-term temporally stable illumination, it simplifies TIRF/HILO imaging, and allows for simple methods of making the illumination homogenous across the FOV. Two types of fibers are generally used for microscopy: single- and multimode. Multimode fibers offer several advantages over single mode fibers: their large core size means they are easy to align and there is negligible loss of laser power. They also maintain alignment over longer periods of time. However, while the output of a single mode fiber is a near-perfect Gaussian profile, a multimode fiber will introduce speckling and a non-uniform profile [40]. It is this property, however, that allows them to be used for homogenizing the illumination over the FOV (Section 2.1.2).

The simplest method for TIRF/HILO imaging with epifluorescence microscopes requires the laser to be focused onto a spot on the back-focal-plane of the objective (BFP) (Fig. 1); the laser will exit the objective collimated. If the spot is translated on the BFP, the angle of the laser beam at the exit of the objective will change, enabling TIRF illumination [35,41]. For HILO [37] an extra mirror is used to adjust the tilt of the spot on the BFP, adjusting the depth of the sheet on the imaged area [42]. Placing a fiber coupler on an XYZ translation stage (available from Thorlabs, Inc. or Newport Corporation) allows the laser spot to easily be focused and translated on the BFP. Free space launching requires a method to adjust the position (and tilt for HILO) of the spot on the BFP: for more information on how to achieve this, see [36,43,44].

Of note, most laser light will be linearly polarized and only molecules which are aligned with the polarization axis of the laser will be excited efficiently. In order to excite all molecules present in the sample, the laser light should be converted from linearly polarized to circularly polarized [39], which can be achieved by placing a quarter-wave plate in the light path [45]. Another point to consider is that back-reflections of the laser onto the laser cavity will destabilize the laser. Optical isolators using polarizing optics and reduce this problem but a simpler method is to use angled polished fiber connectors (FC/APC), the reflections of which will not go back through the optical path and into the laser cavity.

### 2.1.2. Large FOV illumination

New sCMOS camera technologies are capable of imaging a  $2048 \times 2048$  pixel FOV at 100 frames per second (FPS). This is in comparison to EMCCD cameras, traditionally used for single molecule imaging due to their high sensitivity [46], which can image a  $512 \times 512$  pixel FOV at a maximum speed of 56 FPS. For example, Soares et al. [30] used an EMCCD to image 1–6 cells for each  $512 \times 512$  pixel FOV. Using the full  $2048 \times 2048$  chip of an sCMOS camera would yield a 15-fold larger area and, therefore, number of cells imaged per FOV. With the doubling of full-frame speed, this corresponds to a 30-fold increase in throughput, a clear advantage of sCMOS cameras for HT SMLM. The large FOV afforded by sCMOS cameras thus makes it important that images are sampled correctly and that the whole FOV is illuminated appropriately.

The total magnification of the system will be the product of the objective magnification (which takes into account the magnification of the tube lens) and any extra magnification present in the system. The size of a pixel in the projected image will be the physical camera pixel size divided by the total magnification. The ideal pixel size for a widefield image should be about  $2.3\times$  smaller than the diffraction-limited resolution of the microscope (according to the Nyquist criterion) [39]. For a 1.4 NA objective imaging a molecule with 525 nm emission, the diffraction-limited resolution is 230 nm and hence the Nyquist pixel size is 100 nm [39]. As a result, whilst an EMCCD camera (with a pixel size of

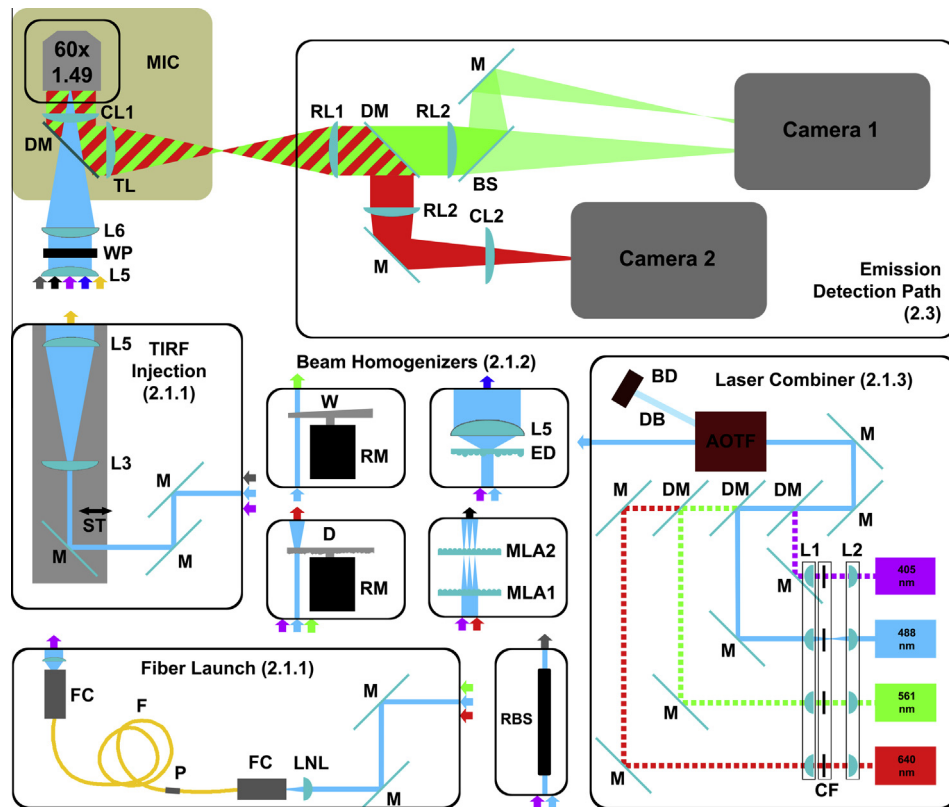


**Fig. 1.** Schematic of the hardware options available. Pictured are the all the major options when assembling a high-speed SMLM microscope. Different colored arrows represent the possible next step in the optical path and numbers in brackets are the corresponding sections in the text. Laser combiner: lasers can be steered with mirrors (M), combined using dichroic mirrors (DM) and either modulated directly or through an AOTF. Of note, the AOTF will output a diffracted beam (DB) which is directed to a beam dump (BD). Also, correcting laser divergence using two lenses with the same focal length (L1 and L2) improves transmittance through fibers and cleanup filters (CF) will minimize background excitation. Beam homogenizers: after the combiner, there are several options to homogenize the beam: a rotation motor (RM) with a wedge (W) or diffuser (D), or a combination of both can be used with a multimode fiber (F); an engineered diffuser (ED) can be used along with a lens to collimate (L5) and another lens (L6) to focus on the BFP inside the microscope (MIC); a set of two microlenses (Koehler integrator) can be used before L5 in order to homogenize the FOV and optionally with a rotating diffuser; a refractive beam shaper (RBS) can be used for TIRF injection and its input can be from a single-mode fiber or directly from the laser combiner (F); or by simply vibrating a multimode fiber (F) with a Piezo element (P) or any other source of high-frequency vibrations. Fiber launch: when using a fiber, the laser beam needs to be focused on the fiber coupler (FC) using a lens with an NA equal to the fiber's (LNL). TIRF injection: TIRF illumination can be achieved by, for example, mounting a mirror, beam expander (divergent lens L3 with collimating lens L5) and L6 on a translating stage (ST) to move the focus of the laser on the BFP. Using a quarter-wave plate (WP) is advised to circularly polarize the laser light. For HILO, a few extra lenses are required: see [42]. Emission detection path: the sample's emission can be split to two cameras, two sides of a single camera or a combination of both. Emission is separated from the excitation using a DM and most microscopes will have a tube lens (TL) placed immediately after. An optical relay is placed two focal lengths away from the TL and consists of two lenses (RL1 and RL2). The emission light can then be split using a DM or a 50/50 beam splitter (BS) (only a DM is shown in the example) which splits the intensity of the light in half, in two directions. The DM or BS can be placed between RL1 and RL2 to split to two cameras or between RL2 and the camera to split to two different halves of the chip. The shown example with a single mirror will introduce focus shifts in the two images, which enables 3D imaging. Alternatively, 3D imaging can be accomplished by placing a 10 m focal length cylindrical lens between the objective and the TL (CL1) or a 1 m focal length lens between RL2 and the camera (CL2).

$16 \times 16 \mu\text{m}^2$ ) typically requires a 100x objective to ensure ideal pixel sampling, an sCMOS camera (pixel size  $6.5 \times 6.5 \mu\text{m}^2$ ) only requires  $63\times$  magnification to satisfy the Nyquist criterion, which allows for imaging of a larger FOV.

When the illuminating laser spot is focused onto the BFP, as used in TIRF/HILO imaging, the intensity distribution of the illumination at the sample will be an image of the beam shape. For most lasers this is Gaussian, or at least non-uniform [41]. This non-uniform power distribution results in different fluorophore dynamics in different parts of the image. To increase illumination homogeneity across the FOV, most SMLM systems illuminate a much larger field than the one being imaged. However, this reduces the laser power density, requiring the laser power to be increased concomitantly. Inhomogeneities across the FOV can also arise from the laser launching method, as launching using multimode fibers introduces intense 'speckles' in the illumination field [40]. For large FOV imaging it is important to achieve a large, homogenous illumination field whilst maintaining suitable on-sample laser power.

Particularly interesting methods for homogenizing illumination involve manipulating the light path as it travels through a

multimode fiber, and such methods have the advantages of negligible power loss and an output suitable for TIRF imaging. While the output of a multimode fiber is inherently uniform ("flat-top"), intense speckles and interference fringes can appear as a result of the coherence of laser light [47,48]. Simple methods for reducing these inhomogeneities involve vibrating, agitating and/or bending a multimode fiber at a relatively small radius (but not small enough to be damaged [49,50]). Provided that the vibration frequency is  $10\times$  higher than the acquisition rate of the camera, different outputs of the fiber will blur together and create a uniform illumination field [50]. As such, piezoelectric elements are typically required to vibrate the fiber [50,51], although in principle any vibration source can be used. For example, beam homogenization has been achieved by coiling a fiber around a laser cooling fan [52]. There are also some fibers with a square output, optimizing the laser illumination to the square area of camera sensors. These fibers are not as easily available as fibers with circular output, however.

In order to implement a vibrating fiber system, a careful choice of multimode fiber and vibrating system is required. For example,

**Table 4**

Qualitative evaluation of homogenization methods. Summary table of all four methods outlined above, highlighting the uniformity of the output, how much laser power is lost by the implementation, whether TIRF is possible, how expensive it is in relation to the other methods and how complex the method is to implement on most modern SMLM systems. MMF – multimode fiber, diff. – diffuser.

Method	Uniformity	Power loss	TIRF	Cost	Complexity
Refractive beam shaper	Excellent	Low	Yes	\$\$\$	Low
Vibrated MMF	Moderate	Low	Yes	\$\$	Moderate
MMF + rotating wedge/diff.	Very good	Moderate	Yes	\$\$	Moderate
Engineered diffuser	Moderate	Moderate	No	\$	Low
Koehler integrator	Very good	High	No	\$\$	High

fibers with large core sizes transmit more modes and are more sensitive to vibrations [45]. The NA of the fiber will also limit the achievable collimation quality of the laser after the fiber-collimating lens. The focal length of this lens and the NA of the fiber will offer a trade-off between size of the beam and its collimation. Of note for multimode fibers, the NA of the lens that focuses the beam onto the fiber should match the NA of the fiber [53]. If the lens NA is too low, there will not be enough speckles generated to be mixed and homogenize, and the beam output will be more Gaussian; if the lens NA is too high the difference from the fiber NA will introduce a power loss proportional to that difference. Also, as the frequency at which the fiber is vibrated limits the maximum imaging frequency over which the FOV remains uniform, piezoelectric elements with resonant frequencies of 20 kHz and 40 kHz (Premier Farnell plc, RS Components, Ltd.) will limit the maximum imaging frequency to 2 kHz and 4 kHz, respectively [50]. However, such imaging frequencies should be sufficient for most SMLM applications. If the amplitudes of vibrations from piezoelectric elements are not sufficient, several piezos may be combined. To reduce speckles, the light path can also be manipulated prior to multimode fiber injection, for example by inserting a spinning glass wedge [47,48] or rotating plastic petri dish [54] into the free space light path; these methods can be combined with a vibrating fiber system if the amplitude of vibrations from piezos are insufficient. Again, spinning or rotation should be performed at a higher frequency than the acquisition rate.

There are other optical methods for homogenizing illumination available. These include refractive beam shapers which output an arbitrarily defined illumination profile [55] (piShaper from AdlOptica Optical Systems GmbH, refractive beam shapers from Newport Corporation) when given a defined input beam, and various diffractive beam shapers such as Koehler Integrators [56–58] (available from RPC Photonics or SÜSS MicroTec AG) and engineered diffusers [59,60]. However, the latter two methods are not suitable for TIRF/HILO as they rely on the creation of multiple laser spots. The refractive beam shapers are very simple to integrate but are expensive and require high-quality beam shapes to avoid losses. A qualitative evaluation of beam homogenization methods is provided in Table 4.

### 2.1.3. Laser choice and modulation for SMLM

To increase the speed of PALM acquisition, cycling of the 405 nm activation laser with the excitation laser required very fast laser modulation [17]. Modern laser microscopes typically use compact solid-state or diode lasers, which have high stability and offer high-frequency direct modulation of laser intensity [39]. If the laser cannot be modulated fast enough, Acousto-Optic Tunable Filters (AOTF) or Acousto-Optic Modulators (AOM) can be used (Fig. 1) [39]: AOMs are used to modulate intensity of a single laser, whereas AOTFs can modulate the intensity of several

lasers in a wavelength selective manner [39]. If the laser can be directly modulated, an AOTF might not be necessary but electronic controllers might be required to modulate the lasers at high-frequency, such as those available from National Instruments Corp., Measurement Computing Corp. or the open-source Arduino platform. If fast dSTORM imaging is to be performed, the 405 nm laser can be continuously present with the excitation laser, making fast modulation unnecessary. However, fast dSTORM imaging requires powerful lasers (laser intensity at the sample in the order of 1–100 kW/cm<sup>2</sup> [32]) since excitation intensity is inversely proportional to “on-times” [16]. For example, Huang et al. [46] use a 500 mW 642 nm laser to illuminate relatively small FOV's to be able to achieve power densities of 5–18 kW/cm<sup>2</sup>. Such lasers are not easily available or cheap, however. Telecommunication laser companies do offer models that can be useful for SMLM; Section 3 mentions a few such companies. High power lasers do however require additional safety considerations and precautions to avoid damage to components. Users should be intimately familiar with the safety recommendations that come with their laser model and sufficient information should be available from the local safety officer. When imaging for long periods these lasers also warm the objective considerably which can damage the coatings of the optics and degrade the cement used for the optical components in the objective. The authors have seen this first-hand after imaging for one hour with all lasers turned on at full power. Taking regular breaks to cool the components should help with longevity.

Another important property of the laser is its beam shape, or the transverse electromagnetic mode (TEM) of the beam. The simplest profile corresponds to a Gaussian distribution, referred to in specifications as TEM<sub>00</sub> [45]. Beams with a TEM<sub>00</sub> profile are preferable for SMLM as they are simpler to homogenize than other modes, and their single peak allows for better definition of the correct illumination angle in TIRF/HILO imaging. The TEM<sub>00</sub> profile can also be achieved by transmitting any laser light through a single-mode fiber [45]. However, the disadvantages of using a single-mode fiber as opposed to a multimode fiber are that extra optics will be required to homogenize the output, and that correctly aligning single-mode fibers is substantially harder with typical power losses of 30–40% [39]. Whilst most SMLM systems simply magnify TEM<sub>00</sub> illumination to a much larger area than the FOV to achieve uniformity, for large FOV illumination the beam homogenization techniques described in Section 2.1.2 are recommended to prevent losing power density at the sample. Beam homogenization also allows for lasers with lower beam quality to be used, reducing costs.

## 2.2. Detection optics and frame

### 2.2.1. Focus drift correction

Regardless of imaging speed, when imaging for several thousands of frames over tens of minutes, sample drift becomes a problem. This is due to different thermal responses between different materials in the microscope body. While lateral drift can be corrected post-acquisition by tracking fiducial markers (such as fluorescent beads) included in the sample, axial drift results in the sample moving out of focus, rendering the acquisition unusable. Axial drift can be addressed via correction or prevention with hardware and/or software solutions. Software solutions rely on motorized focusing systems and a microscopy acquisition package that can stop the acquisition at regular intervals, take images a few microns above and below the current focus, and determine the position of the previous focus. Most commercial acquisition packages offer this, as well as the free and open-source MicroManager microscopy control software [61]. The most common hardware solution is based on integrating an infrared LED light into the

**Table 5**

Comparison of relevant features of modern microscope bodies for custom SMLM systems. We find the ASI RAMM highly versatile and cost-efficient, but their focus system requires some habituation. Access to optics refers to how easily one can modify the excitation and emission paths; dual turret refers to the possibility of adding more than one dichroic cube changer.

	Ti-E	DMi8	IX83	Axio observer	ASI RAMM
Focus correction					
Performance	Best	n/a	Good	Good	Good
Ease of use	Simple	n/a	Reasonable	Reasonable	Learning curve
Access to optics	Good	Good	Good	Poor	Best
Dual turret	Yes	No	Yes	No	Yes
Eyepieces	Yes	Yes	Yes	Yes	No
Cost	\$\$\$	\$\$\$	\$\$\$	\$\$\$	\$\$

microscope light path such that some light is reflected from the interface of the coverslip and sample media. Changes in this signal will indicate when the focus is drifting, and the microscope can then compensate for this by moving the focus by the same amount as the measured drift [62]. Such systems work best when water-based media are used at the interface. This solution is available from the “big four” microscope hardware manufacturers (Table 5) and is offered as an upgrade to modern microscope bodies. Of note, having informally tested several of these systems, we find the Nikon Perfect Focus System to be the best in both simplicity and performance. There are also add-on solutions for older or homebuilt systems such as the Applied Scientific Instrumentation CRISP system or the open-source hardware pgFocus system [63].

### 2.2.2. Accelerating high throughput and multicolor microscopy

High throughput microscopy relies on fast and automated acquisition. The automation is achieved by motorizing the sample stage, illumination and emission capture. Given that a HT microscopy workflow involves repeating the same mechanical movements several hundreds of times, any speed saved on movement significantly increases throughput. All four of the major microscope manufacturers offer fully automated microscopes with different automation options for the same model. At the heart of the HT microscope is the sample stage and most suppliers offer fast XY translation stages. More importantly, the default motorized focusing systems in most bodies are relatively slow; this can be overcome by either adding a piezo translator to move the objective, adding a stage-top piezo Z translator or by purchasing an integrated XYZ piezo stage. Prior Scientific Instruments Ltd., Applied Scientific Instrumentation (ASI), Mad City Labs (MCL) Inc., Physik Instrumente (PI) GmbH & Co. KG are just some of the manufacturers who offer some or all of these options. A stage-top Z translator is a popular option since it can work with multiple objectives (the piezo objective translator can only be mounted on a single objective at a time), it can be mounted on stages which are already present in most microscopes and will have a much larger travel range compared to a XYZ piezo translator.

If multicolor illumination is required, this can also be another bottleneck for speed. In most widefield microscopes separation of different wavelengths is achieved by moving a revolving turret of filter cubes, which include excitation, emission and dichroic filters. These filter cubes typically take a few hundreds of milliseconds to move, which accumulates considerably during the HT microscopy workflow. As laser illumination is used in SMLM, laser selection can be achieved with direct modulation or with an AOTF (delays of milliseconds) and so mechanical changing of excitation filters is unnecessary; a single dichroic which only reflects the laser wavelengths in use is sufficient. However, an excitation clean-up filter in front of the laser itself is advised (Fig. 1) as this will remove any additional unwanted wavelengths emitted by the laser. Although emission filters may also be unnecessary when using spectrally distinct fluorophores, we recommend that an emission

clean-up filter be present before the camera to remove both stray laser reflections and unspecific emission. If emission filters are required (for example when there is fluorophore crosstalk or auto-fluorescence), these can be mounted in motorized filter wheels with switching times of a few tens of milliseconds. These are available from major microscope brand distributors or some of the previously mentioned companies (Prior, ASI). For good quality TIRF, the dichroic mirror should be free from distortion to avoid corrupting the laser focus. Thicker dichroic mirrors suffer less surface stress from being clamped in holders, and thick dichroics glued to holders are available from Chroma Technology Corp.

### 2.3. Detection path for high-speed SMLM

A further method for accelerating multicolor fast SMLM is by using two cameras simultaneously instead of one, or using two sides of the same camera sensor, simultaneously acquiring two different emission spectra from the sample (Fig. 1). Since the acquisition for each color is made in parallel and not sequentially, this results in a doubling of the acquisition speed. Although it should be noted that splitting between two cameras or between different parts of the same camera decreases lateral resolution due to the lower number of photons in each camera (or part of the camera) for localization. Instead of multicolor imaging, these two views can be used for biplane 3D imaging (2.3.1) [64]. Splitting the emitted light into two cameras is greatly simplified if the user has access to the infinity path, which is the collimated light path exiting the BFP of an (infinity corrected) objective [39]. However, modern commercial microscopes do not offer easy access to place a second dichroic and a camera in the limited geometry of the infinity path. An exception is the Rapid Automated Modular Microscope system from ASI imaging, which offers complete access to the optical path.

#### 2.3.1. 3D SMLM

SMLM microscopes can be designed to increase axial (Z) resolution as well as lateral resolution, and techniques for 3D SMLM are typically based on manipulating or knowing the shape of the point spread function (PSF) of the microscope. The PSF describes how a point source of light is imaged by an optical system, and due to diffraction of light by the microscope optics the image is blurred in X, Y and Z; all images made with the microscope can be considered a convolution of the PSF with the real structure of the sample [39]. The PSF size is approximately 3× larger in the Z dimension than in XY, and thus the axial resolution is accordingly poorer than the lateral resolution [39].

Three common methods whereby 3D SMLM images can be reconstructed are biplane imaging [64], astigmatic [65] and double-helix (DH) PSF [66] methods. Biplane imaging takes advantage of the observation that the lateral dimensions of the PSF increase with axial distance from the focus. By taking two images at different known focal positions and measuring the ratio in the

**Table 6**

Qualitative comparison of the mentioned 3D SMLM methods (CL – cylindrical lens; DH-PSF – double helix PSF). Complexity refers to the ease of implementation in custom SMLM systems. Depth of coverage evaluates the axial extent where localization precisions are acceptable; low SNR performance refers to how well the method performs in situations of high background and/or low signal.

	CL	DH-PSF	Biplane
Cost	Low	Moderate	High
Complexity	Low	High	Reasonable
Depth of coverage	Poor	Best	Good
Low SNR performance	Good	Low	Best

differences in the lateral PSF shape, one can determine the relative position of the object in Z [64]. However, as emission light must be split between two cameras, lateral resolution is decreased (as discussed above). Astigmatism and DH are based on shaping the PSF in such a way that its shape will have information on the axial position of the molecule encoded in it, and this position can be extracted post-acquisition from the lateral shape of the PSF [65,67]. Both of these methods require additional optics in the detection path to shape the light: DH requires a spatial light modulator (and often an optical relay) [66] whereas astigmatism only requires a  $f = 1$  m cylindrical lens in front of the camera [68]. If the camera is inaccessible, astigmatism can be achieved by adding a  $f = 10$  m cylindrical lens to the infinity path of the microscope (for example, by inserting the lens into a slider such as that present in the Nikon Ti-E [69]). In both astigmatism and DH the distribution of light over a larger area results in decreased lateral resolution. For comparisons of these methods see Badieirostami et al. [68], Liu and Lidke [70], Mlodzianoski et al. [71] and Table 6.

### 2.3.2. Optical relays

In general, it is not simple to split the emission light between two cameras in a commercial microscope. Commercial options are available, which adapt the regular camera port of microscopes to add two cameras (Andor Technology Ltd. TuCam, Cairn Research Ltd Twincam) or to split the light in two sides of the same camera chip (Cairn Research Ltd. Optosplit II). When using an sCMOS camera the large chip allows splitting without requiring a second camera; while this increases acquisition speed, it sacrifices FOV which is not desirable for high-throughput microscopy.

The commercial splitters are essentially optical relays, which can also be assembled in home-built systems [64,72]. Optical relays consist of two lenses: one is placed after the tube lens to collimate the light, and the other placed in front of the camera to focus the image onto the sensor (Fig. 1). If these two lenses have different focal lengths their ratio will introduce an extra magnification and so care should be taken when calculating the final magnification of the system (Section 2.1.2). The splitting itself is achieved with a dichroic or a 50/50 beam splitter between the two relay lenses to avoid distortions (Fig. 1). When placing the splitting optic between the second lens and the camera, distortion can be minimized by focusing onto the camera with a long focal length lens, such as in the original biplane paper [64].

### 2.3.3. Camera speed considerations

Electronic cameras' sensors acquire a signal by collecting electrons that are generated when a photon hits the sensor. During read-out these electrons are then "read", meaning that the signal is quantified for each pixel and transmitted to the computer. Camera acquisition time is generally limited by the time it takes to read the signal for each exposure. Read-out also introduces some variability into the signal, which manifests as noise in the image (read noise).

Most commercial TIRF microscopes have an EMCCD camera installed, and the read-out speed of an EMCCD can be increased

by enabling the Frame Transfer function, which allows the camera to start acquiring a second image while the first is still being read, or by cropping the detector to a smaller FOV.

However, for fast high-throughput SMLM, sCMOS cameras are ideal as they possess larger chips and are inherently faster than CCD cameras. When the amplification noise of EMCCD cameras is taken into account, sCMOS cameras also have higher quantum efficiencies (the fraction of photons effectively captured by the camera) than EMCCD cameras [73]. As such, sCMOS cameras can surpass the performance of an EMCCD for SMLM. The mechanism through which sCMOS cameras are read out is via a rolling shutter type exposure [74], which results in different parts of a single exposure being imaged at different times. While this can be problematic when imaging objects moving faster than the acquisition rate of the camera, this should not hinder SMLM imaging of fixed samples or live-cell samples where any movement is on a sufficiently slow timescale.

If even faster imaging is required at the expense of FOV, the sCMOS sensor can be cropped as for EMCCDs. However, as each row in an sCMOS sensor has to have all its pixels read, cropping the sensor would only increase speed for each complete row of pixels not read by the camera. This is in contrast to EMCCD cameras, where any cropping will always increase speed.

## 2.4. Acquisition computer

### 2.4.1. Software control of hardware

All controllable hardware associated with the microscope needs to be synchronized during acquisition. Most commercial microscopes offer a software package which is capable of controlling the hardware mentioned so far, but their flexibility will vary. The open source MicroManager software [75] can be used to control almost all models of lasers, cameras and microscopy hardware. It also provides a very flexible beanshell based scripting language which permits a user to control all aspects of data acquisition, plugins for HT microscopy and fast multi-dimensional acquisition.

When using two sCMOS cameras, care needs to be taken to ensure that they are synchronized, otherwise the images will have parts that are time shifted in relation to each other due to the rolling shutter. Synchronization can be achieved by triggering the start of each acquisition at exactly the same time using a transistor-transistor logic (TTL) signal. This can be done by sending a signal from one camera to the other or by sending a signal from an external source to both cameras, however triggering from one camera to the other depends on the triggering properties of the cameras and may not be achievable. External triggering of both cameras is generally preferable for tight synchronization but requires a digital I/O device (such as those available from National Instruments Corp., Measurement Computing Corp. or the open-source Arduino platform) that is capable of digital triggering at the frame rate of acquisition. The software also needs to accept two cameras, or else two independent computers have to be used. MicroManager can be configured to work with two cameras in software triggering mode and also supports digital I/O devices.

### 2.4.2. Data storage considerations for sCMOS cameras

The most sensitive (72% quantum efficiency) sCMOS cameras acquire  $2048 \times 2048$  pixel 16-bit images at 100 frames per second. This corresponds to having to transfer  $\sim 840$  megabytes of data per second (MB/s) to the computer, and a typical SMLM stack of 10,000 to 50,000 frames will require 42–84 gigabytes of memory. Acquisition software such as MicroManager can stream all of this data to either RAM or the hard drives. RAM is fast enough to write the data but generally limited in size and more costly; a hard-disk drive (HDD) is too slow to write but has sufficient storage space

and is cost-effective. Alternatively, Solid State Drives (SSDs) are storage drives which are much faster than HDDs (hundreds of MB/s versus tens of MB/s, performance varying per model) but are also more costly. SSDs (or HDDs) can be multiplexed, where  $x$  drives can work in RAID0 mode to increase speed by a factor of  $x$ , providing more space than RAM at a lower cost. However, a typical SMLM experiment will generally require several tens or hundreds of sets of acquisitions, and HT microscopy could require thousands, and hence it is evident that data storage is a thorny problem in SMLM. Having a direct fiber-optic network connection to a server with large storage capacity is an obvious advantage. Any new system being considered, commercial or home built, must have the requisite IT infrastructure to handle the expected volume of data.

### 2.5. Setting up a space for building a system

In addition to the above hardware and IT infrastructure considerations for constructing a SMLM system, the local environment of the microscope is also important. As SMLM systems require the imaging of single molecules, any high-frequency vibrations present in the system will result in a blurring of the PSF by the amplitude of the vibration, degrading the localization precision. Such vibrations may be present in a system but not visible until imaging is performed at a high frame rate.

There are several ways to minimize vibrations in the system. Firstly, the system can be built on an air-dampened table, which filters vibrations transmitted from the ground. In general, heavier and larger tables will filter vibrations more effectively, and dampening specifications of tables are available from manufacturers (Thorlabs Inc., TMC Mfg., and Newport Corporation). Additionally, there are greater vibrations in higher floors of buildings and as such many SMLM systems are housed in the ground floor or basement of buildings. Any equipment which could cause vibrations should also be on separate tables; computers should be placed away from the system, preferably on rubber feet, and laser fan vibrations can be avoided by placing lasers on a separate table and using optical fibers to deliver beams to the main table. Alternatively, water cooling systems may be used instead of the inbuilt fans in lasers and cameras.

Maintaining an appropriate temperature in the microscope room is also important. As most modern optics and immersion oils are optimized for a room temperature of 23 Celsius, care should be taken to ensure that the air-conditioning maintains this temperature on the microscope. To achieve this, it may be necessary to lower the set point of the air conditioning to a slightly lower temperature to negate heat generated by components of the microscope. Thermal stability in the microscope room is crucial for minimizing drift; we have seen in practice that although drift is noticeable in the first few minutes after placing the sample, after this period drift becomes negligible in a thermally stable room. Systems for correcting residual focal drift are discussed in Section 2.2.1, and any residual lateral drift can be easily corrected for computationally by including reference markers (such as fluorescent beads or gold nanoparticles) in the sample [12]. Most commercial and open-source SMLM localization software such as QuickPALM [76] have integrated drift correction algorithms based on tracking these reference markers. For temperature and environmental control in live cell imaging, additional hardware such as incubation chambers are required; these are beyond the scope of this review but are reviewed elsewhere in a non-SMLM context [77].

The system should also possess suitable shielding from stray photons, as these will increase background noise and decrease the SNR. There are black-out boxes available for almost all commercial systems (Pecon GmbH), and for homebuilt systems

darkening the walls will also allow for easy identification of stray laser reflections and will thus aid alignment.

Electrical stability is also important. Fluctuations in power supplies may affect the performance of lasers and electronic devices such as AOTFs and piezo stages. Using an Uninterrupted Power Supply (UPS) unit is always recommended, as it will stabilize the electrical system associated with the SMLM components and protect the devices from power spikes and blackouts.

### 2.6. Analytics for sCMOS camera acquisitions

#### 2.6.1. sCMOS noise patterning problem

While there is freely available software for SMLM analysis such as QuickPALM [76], ThunderSTORM [78] and RapidSTORM [79], these all assume acquisition with an EMCCD camera. As such these programs may not be suitable for analyzing data acquired with sCMOS cameras, as each pixel in an sCMOS chip has its own noise properties [46] and hence SMLM localizations may be biased toward high-noise pixels. Although manufacturers include a correction on the camera chip for this, the correction methods are not published and may not remove the localization bias. However, Huan et al. have published a method for correcting this bias [46], which involves characterizing pixel noise obtained from several thousands of dark frames, and SMLM software with corrections for noise patterning is provided on their website [80].

#### 2.6.2. Impact of analysis algorithms on acquisition speed

As discussed previously, a limiting factor in SMLM acquisition time is ensuring that a sufficient number of molecules are localized to reconstruct the labeled structures. A simple way to decrease total acquisition time is to increase the density of on-state molecules per frame, reducing the number of frames required to yield the same total number of localizations. A further advantage is that lower laser intensities (or even lamp-based illumination [81]), can be used for higher density acquisitions (Section 1.1). However, when acquiring at higher densities, fluorophores start to overlap and cannot be distinguished by traditional SMLM algorithms. Specialist algorithms have been developed which can handle high-density datasets [81–85], with some methods capable of reconstructing from a few hundreds of frames. High-density methods are particularly relevant for HT microscopy as they also reduce data processing and storage hardware requirements.

There are currently three prominent high-density algorithms. Bayesian Localization Microscopy (3B) has been used to perform live imaging of podosomes at 50 nm resolution with a simple widefield microscope, requiring only a few seconds of acquisition time (200 frames). The drawback of this method is that it is computationally intensive (6 h for a  $1.5 \times 1.5 \mu\text{m}^2$  area), however the software is freely available [81]. Compressed Sensing STORM is an algorithm that has been demonstrated to reconstruct 60 nm resolution images of microtubules from 169 frames [85], and the Matlab code is available with the paper. As with 3B, this method is computationally demanding and one group reported taking a whole day to process a  $100 \mu\text{m}^2$  region [83]. Stochastic Optical Fluctuation Imaging (SOFI) is capable of doubling the resolution with a standard widefield microscope (200 frames) [86] and achieving 80 nm resolution with a TIRF microscope with low laser powers (5000 frames) [87]. The virtual removal of background and out-of-focus light in SOFI allows it to generate optically sectioned z-stacks, and a Matlab SOFI package is freely available SOFI package [88]. However, SOFI image interpretation is artifact prone as resultant image intensity is representative of temporal optical fluctuations and not original signal intensity, so gaps can emerge in areas where the intensity did not fluctuate sufficiently. While these high density algorithms may require high computational intensity

or produce some artifacts, the increase in speed afforded by high density acquisition is still sufficiently worthwhile.

### 3. Putting it all together

So far we have described several of the design options for a high-speed high-throughput SMLM system with an sCMOS camera. Perhaps the most important decision will be whether or not a TIRF objective is used, as this will limit the size of the uniform FOV and hence the maximum area of the sCMOS chip that will yield usable data. TIRF can however still be achieved (with an added degree of difficulty) using 1.4 NA non-TIRF specific objectives when imaging samples in water-based media [16,89].

For high-throughput and large FOV imaging, beam homogenization is recommended to increase the uniformity of the FOV. A vibrating fiber system is perhaps the most efficient method of those described in Section 2.1.2 and is relatively simple to implement. Refractive beam shapers are also simple and effective optics for beam homogenization, but are more costly than other methods.

Further options for enhancing the versatility of the system for various applications have also been discussed, such as splitting the emission in half (Section 2.3.2). This enables fast multicolor imaging or biplane imaging for 3D SMLM [68,70,71], although if this is achieved by using two halves of the same camera then this reduces the FOV.

There is room for variation on the final system design, depending on the purpose of the system and the context in which it is to operate. To demonstrate this we will outline two possible systems with different properties: (A) an easily assembled system with mostly commercial parts and (B) a low-cost, high-speed system.

#### 3.1. An easily assembled system with mostly commercial parts

Modern, motorized microscope bodies such as the Nikon Ti-E, Olympus IX83, Leica DMI8 or Zeiss Axio Observer offer the most important features required for high-speed or HT SMLM: a hardware drift correction system, motorized focus and well-corrected optics. MicroManager can be used to control any two cameras simultaneously (sCMOS or EMCCD), as well as all of the mentioned stages, laser systems and microscopes in the system described here.

The Andor TuCam adapter can be used with any of these systems to allow for imaging in two sCMOS cameras, such as the Hamamatsu Flash 4.0 or Andor Zyla 4.2. To obtain 100 nm pixels (to satisfy the Nyquist sampling criterion as discussed in Section 2.1.2) while using the whole FOV and TIRF illumination in water-fiber-coupled output and fast modulation, which can be used with no additional magnification in components such as camera adapters.

In order to reduce complexity and provide warranty coverage, complete turn-key laser assemblies which contain several lasers coupled together can be obtained from several manufacturers (Omicron-Laserage Laserprodukte GmbH, TOPTICA Photonics AG, Oxixus SA, Vortran Laser Technology, Inc.). All of these offer a TEM00 fiber-coupled output and fast modulation, which can be directly controlled with MicroManager. However, the laser powers in commercial turn-key systems may be limited compared to custom laser systems.

The most challenging part of the system to assemble is the laser launching and beam homogenization system. The simplest high-efficiency method to homogenize the laser illumination is by using a refractive beam shaper such as the piShaper apparatus, which will convert a 6 mm diameter Gaussian beam into a 6 mm homogenized beam [90]. A single mode fiber possessing a Gaussian output [45] can be used to inject the laser beam into

the piShaper. Launching through a fiber will also increase the stability of the system and allow for lasers (and their vibrations) to be located away from the optical table. As the output of a fiber is divergent, it must be collimated using a plano-convex lens, and the resultant beam size depends on the focal length of the lens  $f$  and the numerical aperture of the fiber NA as  $2^*f*NA$  [91]. For example, to obtain a collimated 6 mm beam to input into the piShaper from a 0.12 NA single mode fiber (S405-XP, ThorLabs), an achromatic 25 mm lens is required (AC127-025-A-ML, Thorlabs).

Similarly, the 6 mm uniform output of the piShaper must be expanded to match the 19 mm diagonal size of the Flash 4.0 and Zyla 4.2 cameras (of note, this is only the case when not changing the magnification before the camera and when the lens to focus on the BFP has the same focal length as the tube lens [36]). This can be achieved using a two-lens Galilean beam expander (which introduces minimal chromatic aberrations [49]) where the ratio of the two focal lengths equals the desired expansion. For example, to expand the 6 mm piShaper output to 19 mm, the output can pass through a  $-50$  mm plano-concave lens (Thorlabs, LC1715-A) and then a 175 mm plano-convex lens (Thorlabs, LA1229-A). Importantly, the expected on-sample power density from a given laser system should be calculated by first multiplying the power ratings with the transmissions from the beam shaping optics and the objective transmission. This will yield the expected on-sample laser power, which must be divided by the area to image; depending on the laser power, it may be necessary to reduce the FOV to reach power densities at least in the few  $\text{kW}/\text{cm}^2$ . Lin et al. [32] provide useful guidelines to determine the necessary powers given a maximum camera frame rate (determined by the size of the FOV), keeping in mind that for HT it is always useful to maximize the FOV. The entire laser launching and homogenization assembly (Fig. 2A) can be mounted on a motorized or manual XYZ stage assembly (Thorlabs and Newport offer many options) to focus the spot on the BFP and translate it in order to achieve TIRF.

Both the Nikon Ti-E and Olympus IX83 bodies offer the possibility of a second dichroic turret for use with laser illumination: this allows for a separate fluorescence lamp or LED illuminator to be used for inspection of the sample through the eyepieces in addition to the TIRF illumination system. The Leica DMI8 also has a secondary illumination port which can be selected by manually moving a mirror; while this system is simpler and cheaper than the Nikon and Olympus systems, the stability of the manual mirror is yet to be fully assessed, and switching between a laser and lamp/LED cannot be automated. As far as we are aware there is no easy way to couple a custom laser launch into the Zeiss system without fully replacing the existing lamp/LED system.

#### 3.2. A low-cost, high-speed HT SMLM microscope

The commercial system described above contains several expensive components; however, low-cost SMLM systems can also be readily constructed. Holm et al. [92] recently demonstrated a simple, low cost system using cheap components. For high-speed HT SMLM most existing microscope bodies can be adapted by coupling an homogenized laser source and installing an sCMOS camera. Although older microscopes will lack focal drift correction, a combination of imaging at sufficiently high speed, high-density acquisition and using a thermally stable room will minimize drift; any residual drift experienced may be corrected for by software autofocus algorithms (such as those present in MicroManager).

For single-color dSTORM imaging, which may be sufficient for most researchers, a single laser will suffice. Alexa647 and Cy5 are generally the best-performing dyes for dSTORM imaging [24] and lasers of appropriate wavelengths can be procured at a reasonable

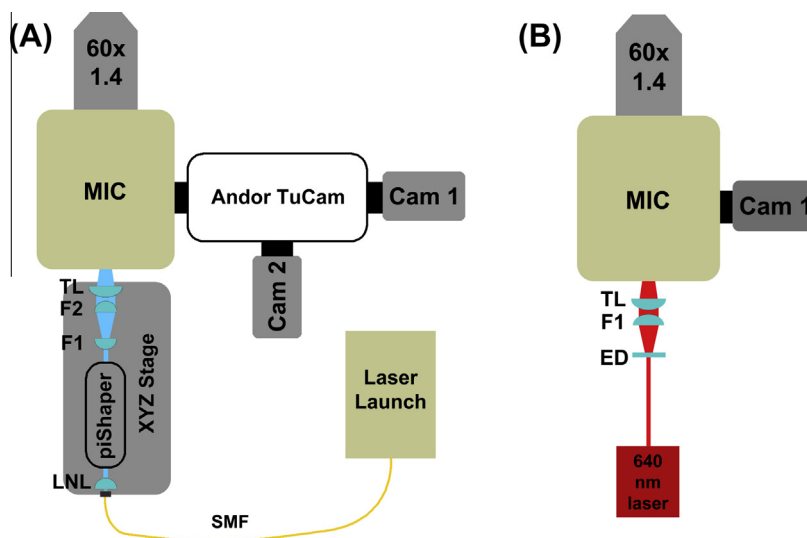


**Fig. 2.** Example systems. (A) An example system built of mostly commercial parts. TL, Tube lens; F1, plano-concave-50 mm focal length lens (Thorlabs, LC1715-A); F2, plano-convex 175 mm focal length lens (Thorlabs, LA1229-A); LNL, collimating achromatic 25 mm lens (AC127-025-A-ML, Thorlabs); XYZ stage, manual translation stage assembly (LNR25D/M and LNR25P2, Thorlabs); MIC, microscope. (B) A low-cost microscope. F1, 60 mm plano-convex focal length lens (LA1134-A, Thorlabs); ED, 20° engineered diffuser (ED1-C20-MD, Thorlabs).

cost (MPB Communications Inc., Shanghai Dream Lasers Technology Co., Ltd., Kvant s.r.o., CNI Laser). Modulation of laser power can be achieved manually using variable neutral density filters (Thorlabs, Inc. Newport Corporation) or digitally using low cost electronic prototyping systems such as the Arduino Due.

For beam homogenization, the cheapest approach may be to use an engineered diffuser, although TIRF is not possible with this method. The laser beam can be input directly onto the diffuser with the output then collimated and focused onto the BFP (Fig. 2B). The diameter of the collimated output is given by  $f \tan \alpha$ , where  $f$  is the focal length of the collimating lens and  $\alpha$  is the output angle of the diffuser [93]. For example, to create a homogenized beam of diameter 19 mm to match the camera chip size (as discussed for the commercial system above), a diffuser with 20° output (ED1-C20-MD, Thorlabs) can be used in conjunction with a 60 mm lens (LA1134-A, Thorlabs). A second lens can then be used to focus this beam onto the BFP. We remind readers to take power density into consideration when choosing a laser and size of the FOV at the sample (see Section 3.1).

This simple, low-cost implementation provides a system that can efficiently illuminate the large FOV of a sCMOS camera, enabling high-speed HT SMLM of the whole FOV.

#### 4. Discussion and future trends in HT SMLM

We have introduced the reader to the hardware options and design caveats when assembling or adapting a microscope for HT SMLM. We hope that this information serves as a basis for more groups to start pushing SMLM into high-throughput. SMLM shows promise in offering better ways to tease out signaling interactions as shown recently [30]. In particular, we have explained factors to be considered when extending SMLM systems for high-speed, large FOV acquisition, with obvious implications for HT microscopy. Most of these considerations revolve around taking advantage of the high speed of sCMOS cameras and their larger chips. These cameras are relatively new to the scientific market and we expect manufacturers to already be improving electronics to increase dynamic range, read out speed and lower noise characteristics. Their large size also means that microscope optic manufacturers need to start adapting their products to this new technology. “Plan” classifications for TIRF objectives that do not cover the

whole FOV need to be reviewed and better corrected, high numerical aperture objectives are imperative to take advantage of these cameras. Regardless, software corrections for aberrations across the FOV should become common features of these cameras and we expect these to become widely integrated in commercial and open-source SMLM software.

More importantly, new reconstruction algorithms are being developed which require fewer frames, can be computed in a reasonable amount of time and can handle large numbers of overlapping fluorophores. These algorithms are set to revolutionize the field since sample, hardware and IT infrastructure requirements are greatly reduced, facilitating HT SMLM as well as live-cell imaging as a routinely feasible proposition for SMLM. Reducing the need to invest in expensive and specialist hardware will hopefully result in widespread adoption and greater development of SMLM, which is a necessary step to move the field to HT. This will not happen, however, if localization reconstruction algorithms are not made available in a simple and widely available manner and it is our belief the future will lie on those who make their source code freely available and compatible with free image processing packages for the life sciences such as Fiji [94]. Likewise, a wider understanding of the hardware underlying these systems is necessary to spread adoption of SMLM and foster its development. We hope that the guidelines laid in this work serve as a starting point for many labs.

#### Acknowledgments

We would like to thank Alan Lowe and Pedro Pereira for their assistance revising the manuscript. PA is supported by a PhD fellowship from the UK’s Biotechnology and Biological Sciences Research Council, SC’s post-doc fellowship is supported by the UK’s Medical Research Council.

#### References

- [1] J. Rino, J. Braga, R. Henriques, M. Carmo-Fonseca, *Int. J. Dev. Biol.* 53 (2009) 1569–1579, <http://dx.doi.org/10.1387/ijdb.072351jr>.
- [2] E. Abbe, *Arch. Für Mikroskopische Anat.* 9 (1873) 413–418, <http://dx.doi.org/10.1007/BF02956173>.
- [3] R. Henriques, C. Griffiths, E.H. Rego, M.M. Mhlanga, E. Hesper, *Biopolymers* 95 (2011) 322–331, <http://dx.doi.org/10.1002/bip.21586>.

- [4] H.H. Rose, *Sci. Technol. Adv. Mater.* 9 (2008) 014107, <http://dx.doi.org/10.1088/0031-8949/9/1/014107>.
- [5] R.H. Wade, *Mol. Biotechnol.* 43 (2009) 177–191, <http://dx.doi.org/10.1007/s12033-009-9193-5>.
- [6] P.J.J. Robinson, L. Fairall, V.A.T. Huynh, D. Rhodes, *Proc. Natl. Acad. Sci. U.S.A.* 103 (2006) 6506–6511, <http://dx.doi.org/10.1073/pnas.0601212103>.
- [7] K.R. Bruce-Alberts, A. Johnson, J. Lewis, M. Raff, P. Walter, *Molecular Biology of the Cell*, 4th ed., Garland Science, New York, 2002.
- [8] S.W. Hell, J. Wichmann, *Opt. Lett.* 19 (1994) 780–782, <http://dx.doi.org/10.1364/OL.19.000780>.
- [9] M.G. Gustafsson, *J. Microsc.* 198 (2000) 82–87, <http://dx.doi.org/10.1046/j.1365-2818.2000.00710.x>.
- [10] E. Betzig, G.H. Patterson, R. Sougrat, O.W. Lindwasser, S. Olenych, J.S. Bonifacino, et al., *Science* 313 (2006) 1642–1645, <http://dx.doi.org/10.1126/science.1127344>.
- [11] S.T. Hess, T.P.K. Girirajan, M.D. Mason, *Biophys. J.* 91 (2006) 4258–4272, <http://dx.doi.org/10.1529/biophysj.106.091116>.
- [12] M.J. Rust, M. Bates, X. Zhuang, *Nat. Methods* 3 (2006) 793–795, <http://dx.doi.org/10.1038/nmeth929>.
- [13] S. Cox, *Dev. Biol.* (2014) 1–7, <http://dx.doi.org/10.1016/j.ydbio.2014.11.025>.
- [14] S. Herbert, H. Soares, C. Zimmer, R. Henriques, *Microsc. Microanal.* 18 (2012) 1419–1429, <http://dx.doi.org/10.1017/S1431927612013347>.
- [15] R.E. Thompson, D.R. Larson, W.W. Webb, *Biophys. J.* 82 (2002) 2775–2783, [http://dx.doi.org/10.1016/S0006-3495\(02\)75618-X](http://dx.doi.org/10.1016/S0006-3495(02)75618-X).
- [16] S. van de Linde, A. Löschberger, T. Klein, M. Heidbreder, S. Wolter, M. Heilemann, et al., *Nat. Protoc.* 6 (2011) 991–1009, <http://dx.doi.org/10.1038/nprot.2011.336>.
- [17] R. Henriques, M.M. Mhlanga, *Biotechnol. J.* 4 (2009) 846–857, <http://dx.doi.org/10.1002/biot.200900024>.
- [18] M. Bates, T.R. Blosser, X. Zhuang, *Phys. Rev. Lett.* 94 (2005) 108101, <http://dx.doi.org/10.1103/PhysRevLett.94.108101>.
- [19] S. van de Linde, I. Krstić, T. Prisner, S. Doose, M. Heilemann, M. Sauer, *Photochem. Photobiol. Sci.* 10 (2011) 499–506, <http://dx.doi.org/10.1039/c0pp00317d>.
- [20] G.T. Dempsey, M. Bates, W.E. Kowtoniuk, D.R. Liu, R.Y. Tsien, X. Zhuang, *J. Am. Chem. Soc.* 131 (2009) 18192–18193, <http://dx.doi.org/10.1021/ja904588g>.
- [21] M. Heilemann, S. van de Linde, M. Schüttelpe, R. Kasper, B. Seefeldt, A. Mukherjee, et al., *Angew. Chem. Int. Ed. Engl.* 47 (2008) 6172–6176, <http://dx.doi.org/10.1002/anie.200802376>.
- [22] J.C. Vaughan, G.T. Dempsey, E. Sun, X. Zhuang, *J. Am. Chem. Soc.* 135 (2013) 1197–1200, <http://dx.doi.org/10.1021/ja31305279>.
- [23] J. Vogelsang, R. Kasper, C. Steinhauer, B. Person, M. Heilemann, M. Sauer, et al., *Angew. Chem. Int. Ed. Engl.* 47 (2008) 5465–5469, <http://dx.doi.org/10.1002/anie.200801518>.
- [24] G.T. Dempsey, J.C. Vaughan, K.H. Chen, M. Bates, X. Zhuang, *Nat. Methods* 8 (2011) 1027–1036, <http://dx.doi.org/10.1038/nmeth.1768>.
- [25] J. Lippincott-Schwartz, G.H. Patterson, *Trends Cell Biol.* 19 (2009) 555–565, <http://dx.doi.org/10.1016/j.tcb.2009.09.003>.
- [26] C. Geisler, A. Schönle, C. von Middendorff, H. Bock, C. Eggeling, A. Egner, et al., *Appl. Phys. A* 88 (2007) 223–226, <http://dx.doi.org/10.1007/s00339-007-4144-0>.
- [27] V. Westphal, S.O. Rizzoli, M.A. Lauterbach, D. Kamin, R. Jahn, S.W. Hell, *Science* 320 (2008) 246–249, <http://dx.doi.org/10.1126/science.1154228>.
- [28] F. Bergermann, L. Alber, S.J. Sahl, J. Engelhardt, S.W. Hell, *Opt. Express* 23 (2015) 211, <http://dx.doi.org/10.1364/OE.23.000211>.
- [29] S.J. Holden, T. Pengo, K.L. Meibom, C. Fernandez, *Proc. Natl. Acad. Sci. U.S.A.* 111 (2014) 4566–4571, <http://dx.doi.org/10.1073/pnas.1313368111>.
- [30] H. Soares, R. Henriques, M. Sachse, L. Ventimiglia, M.A. Alonso, C. Zimmer, et al., *J. Exp. Med.* 210 (2013) 2415–2433, <http://dx.doi.org/10.1084/jem.20130150>.
- [31] A. Egner, C. Geisler, C. von Middendorff, H. Bock, D. Wenzel, R. Medda, et al., *Biophys. J.* 93 (2007) 3285–3290, <http://dx.doi.org/10.1529/biophysj.107.112201>.
- [32] Y. Lin, J.J. Long, F. Huang, W.C. Duim, S. Kirschbaum, Y. Zhang, et al., *PLoS One* 10 (2015) e0128135, <http://dx.doi.org/10.1371/journal.pone.0128135>.
- [33] D. Axelrod, *J. Cell Biol.* 89 (1981) 141–145, <http://dx.doi.org/10.1083/jcb.89.1.141>.
- [34] K.N. Fish, Total internal reflection fluorescence (TIRF) microscopy, *Curr. Protoc. Cytom* (Chapter 12 (2009) Unit12.18), doi:<http://dx.doi.org/10.1002/0471142956.cy1218s50>.
- [35] A.L. Mattheyses, S.M. Simon, J.Z. Rappoport, *J. Cell Sci.* 123 (2010) 3621–3628, <http://dx.doi.org/10.1242/jcs.056218>.
- [36] D.S. Johnson, J.K. Jaiswal, S. Simon, *Curr. Protoc. Cytometry* (2012) 1–19, <http://dx.doi.org/10.1002/0471142956.cy1229s61>.
- [37] M. Tokunaga, N. Imamoto, K. Sakata-Sogawa, *Nat. Methods* 5 (2008) 159–161, <http://dx.doi.org/10.1038/nmeth1171>.
- [38] ISO 19012-1:2013, *Microscopes – designation of microscope objectives – part 1: flatness of field/Plan*, (n.d.), [http://www.iso.org/iso/catalogue\\_detail.htm?csnumber=61652](http://www.iso.org/iso/catalogue_detail.htm?csnumber=61652) (accessed 2.02.15).
- [39] J.B. Pawley, *Handbook of biological confocal microscopy*, 3rd ed., Springer, US, Boston, MA, 2006, doi:<http://dx.doi.org/10.1007/978-0-387-45524-2>.
- [40] J.W. Goodman, *Speckle Phenomena in Optics: Theory and Applications*, Roberts & Company, 2007, doi:<http://dx.doi.org/10.9781936221141>.
- [41] a.L. Stout, D. Axelrod, Evanescent field excitation of fluorescence by epillumination microscopy, *Appl. Opt.* 28 (1989) 5237–5242, <http://dx.doi.org/10.1364/AO.28.005237>.
- [42] J. Sinkó, G. Szabó, M. Erdélyi, *Opt. Express* 22 (2014) 18940, <http://dx.doi.org/10.1364/OE.22.018940>.
- [43] J.L. Ross, R. Dixit, *Methods Cell Biol.* 95 (2010) 521–542, [http://dx.doi.org/10.1016/S0091-679X\(10\)95026-7](http://dx.doi.org/10.1016/S0091-679X(10)95026-7).
- [44] R. Fiolka, Y. Belyaev, H. Ewers, A. Stemmer, *Microsc. Res. Tech.* 71 (2008) 45–50, <http://dx.doi.org/10.1002/jemt.20527>.
- [45] L.M.P., L.S.P., Frank L. Pedrotti, *Introduction to optics*, 2nd ed., Prentice Hall, 1992.
- [46] F. Huang, T.M.P. Hartwich, F.E. Rivera-Molina, Y. Lin, W.C. Duim, J.J. Long, et al., *Nat. Methods* 10 (2013) 653–658, <http://dx.doi.org/10.1038/nmeth.2488>.
- [47] A.L. Mattheyses, K. Shaw, D. Axelrod, *Microsc. Res. Tech.* 69 (2006) 642–647, <http://dx.doi.org/10.1002/jemt.20334>.
- [48] R. Hard, R. Zeh, R.D. Allen, *J. Cell Sci.* 23 (1977) 335–343.
- [49] S. Inoué, K.R. Spring, *Video Microscopy: The Fundamentals*, Springer, 1997.
- [50] Y. Fujimaki, H. Taniguchi, Reduction of speckle contrast in multimode fibers using piezoelectric vibrator, in: A.V. Kudryashov, A.H. Paxton, V.S. Ilchenko, L. Aschke, K. Washio (eds.), 2014, 89601S, doi:<http://dx.doi.org/10.1117/12.2037431>.
- [51] W. Ha, S. Lee, Y. Jung, J.K. Kim, K. Oh, *Opt. Express* 17 (2009) 17536–17546, <http://dx.doi.org/10.1364/OE.17.017536>.
- [52] B. Flamion, P.M. Bungay, C.C. Gibson, K.R. Spring, *Biophys. J.* 60 (1991) 1229–1242, [http://dx.doi.org/10.1016/S0006-3495\(91\)82157-9](http://dx.doi.org/10.1016/S0006-3495(91)82157-9).
- [53] A. Shukla, *Elements of Optical Communication and Opto Electronics*, 1st ed., University Science Press, New Delhi, 2012.
- [54] J.R. Kuhn, T.D. Pollard, *Biophys. J.* 88 (2005) 1387–1402, <http://dx.doi.org/10.1529/biophysj.104.047399>.
- [55] A. Laskin, A.S. Shcherbakov, V. Molchanov, V. Laskin, O. Makarov, *Int. Comm. Opt. Light Dev. World* 8011 (2011) 1–6, <http://dx.doi.org/10.1117/12.901944>.
- [56] S. Herbert, R. Henriques, *Cytometry A* 81 (2012) 278–280, <http://dx.doi.org/10.1002/cyto.a.21177>.
- [57] F.a.W. Coumans, E. van der Pol, L.W.M.M. Terstappen, Flat-top illumination profile in an epifluorescence microscope by dual microlens arrays, *Cytometry A* 81 (2012) 324–331, <http://dx.doi.org/10.1002/cyto.a.22029>.
- [58] R. Völkel, K.J. Weible, Laser beam homogenizing: limitations and constraints, *Proc. SPIE*, 7102 (2008), 71020J–71020J–12, doi:<http://dx.doi.org/10.1117/12.799400>.
- [59] P. Bonifazi, F. Difato, P. Massobrio, G.L. Breschi, V. Pasquale, T. Levi, et al., In vitro large-scale experimental and theoretical studies for the realization of bi-directional brain-prostheses, *Front. Neural Circuits* 7 (2013) 40, <http://dx.doi.org/10.3389/fncir.2013.00040>.
- [60] T.R.M. Sales, *Opt. Eng.* 42 (2003) 3084, <http://dx.doi.org/10.1117/1.1618817>.
- [61] A. Edelstein, N. Amodaj, K. Hoover, R. Vale, N. Stuurman, Computer control of microscopes using µManager, *Curr. Protoc. Mol. Biol.* (Chapter 14 (2010) Unit14.20), doi:<http://dx.doi.org/10.1002/0471142727.mb1420s92>.
- [62] T. Wöllert, G.M. Langford, *Methods Mol. Biol.* 586 (2009) 3–21, <http://dx.doi.org/10.1007/978-1-60761-376-3>.
- [63] PgFocus – BIG-Wiki, (n.d.), <http://big.umassmed.edu/wiki/index.php/PgFocus> (accessed 26.01.15).
- [64] M.F. Juette, T.J. Gould, M.D. Lessard, M.J. Mlodzianoski, B.S. Naggpure, B.T. Bennett, et al., *Nat. Methods* 5 (2008) 527–529, <http://dx.doi.org/10.1038/nmeth.1211>.
- [65] B. Huang, W. Wang, M. Bates, X. Zhuang, *Science* 319 (2008) 810–813, <http://dx.doi.org/10.1126/science.1153529>.
- [66] S.R.P. Pavani, M.A. Thompson, J.S. Biteen, S.J. Lord, N. Liu, R.J. Twieg, et al., *Proc. Natl. Acad. Sci. U.S.A.* 106 (2009) 2995–2999, <http://dx.doi.org/10.1073/pnas.0900245106>.
- [67] M.D. Lew, M.A. Thompson, M. Badieirostami, W.E. Moerner, In vivo three-dimensional superresolution fluorescence tracking using a double-helix point spread function, *Proc. Soc. Photo Opt. Instrum. Eng.* 7571 (2010) 75710Z, <http://dx.doi.org/10.1117/12.842608>.
- [68] M. Badieirostami, M.D. Lew, *Appl. Phys. Lett.* 97 (2010) 161103, <http://dx.doi.org/10.1063/1.3499652>.
- [69] R. Henriques, Tutorial\_Astigmatism – quickpalm, (n.d.), [https://code.google.com/p/quickpalm/wiki/Tutorial\\_Astigmatism](https://code.google.com/p/quickpalm/wiki/Tutorial_Astigmatism) (accessed 27.01.15).
- [70] S. Liu, *ChemPhysChem* 15 (2014) 696–704, <http://dx.doi.org/10.1002/cphc.201300758>.
- [71] M.J. Mlodzianoski, M.F. Juette, G.L. Beane, J. Bewersdorff, *Opt. Express* 17 (2009) 8264–8277, <http://dx.doi.org/10.1364/OE.17.008264>.
- [72] I. Testa, C.A. Wurm, R. Medda, E. Rothermel, C. Von Middendorff, J. Fölling, et al., *Biophys. J.* 99 (2010) 2686–2694, <http://dx.doi.org/10.1016/j.bpj.2010.08.012>.
- [73] F. Long, S. Zeng, Z.-L. Huang, *Opt. Express* 20 (2012) 17741, <http://dx.doi.org/10.1364/OE.20.017741>.
- [74] C.K. Liang, L.W. Chang, H.H. Chen, *IEEE Trans. Image Process.* 17 (2008) 1323–1330, <http://dx.doi.org/10.1109/TIP.2008.925384>.
- [75] A.D. Edelstein, *J. Biol. Methods* 1 (2014) 1–10, <http://dx.doi.org/10.14440/jbm.2014.36>.
- [76] R. Henriques, M. Lelek, E.F. Fornasiero, F. Valtorta, C. Zimmer, M.M. Mhlanga, *Nat. Methods* 7 (2010) 339–340, <http://dx.doi.org/10.1038/nmeth0510-339>.
- [77] M.M. Frigault, J. Lacoste, J.L. Swift, C.M. Brown, *J. Cell Sci.* 122 (2009) 753–767, <http://dx.doi.org/10.1242/jcs.038387>.
- [78] M. Ovesný, P. Křížek, J. Borkovec, Z. Svindrych, G.M. Hagen, *Bioinformatics* (2014), <http://dx.doi.org/10.1093/bioinformatics/btu202>.
- [79] S. Wolter, A. Löschberger, T. Holm, S. Aufmkolk, M.-C. Dabauvalle, S. van de Linde, et al., *Nat. Methods* 9 (2012) 1040–1041, <http://dx.doi.org/10.1038/nmeth.2224>.

- [80] ZhuangLab/storm-analysis GitHub, (n.d.). <https://github.com/ZhuangLab/storm-analysis> (accessed 10.03.15).
- [81] S. Cox, E. Rosten, J. Monypenny, T. Jovanovic-Talman, D.T. Burnette, J. Lippincott-Schwartz, et al., *Nat. Methods* 9 (2011) 195–200, <http://dx.doi.org/10.1038/nmeth.1812>.
- [82] T. Dertinger, R. Colyer, G. Iyer, S. Weiss, J. Enderlein, *Proc. Natl. Acad. Sci. U.S.A.* 106 (2009) 22287–22292, <http://dx.doi.org/10.1073/pnas.0907866106>.
- [83] J. Min, C. Vonesch, H. Kirshner, L. Carlini, N. Olivier, S. Holden, et al., FALCON: fast and unbiased reconstruction of high-density super-resolution microscopy data, *Sci. Rep.* 4 (2014) 4577, <http://dx.doi.org/10.1038/srep04577>.
- [84] E.A. Mukamel, H. Babcock, X. Zhuang, *Biophys. J.* 102 (2012) 2391–2400, <http://dx.doi.org/10.1016/j.bpj.2012.03.070>.
- [85] L. Zhu, W. Zhang, D. Elnatan, B. Huang, *Nat. Methods* (2012), <http://dx.doi.org/10.1038/nmeth.1978>.
- [86] S. Geissbuehler, C. Dellagiacoma, T. Lasser, *Biomed. Opt. Express* 2 (2011) 408–420, <http://dx.doi.org/10.1364/BOE.2.000408>.
- [87] S. Geissbuehler, N.L. Bocchio, C. Dellagiacoma, C. Berclaz, M. Leutenegger, T. Lasser, *Opt. Nanoscopy* 1 (2012) 4, <http://dx.doi.org/10.1186/2192-2853-1-4>.
- [88] Balanced super-resolution optical fluctuation imaging, (n.d.). <http://documents.epfl.ch/users/l/le/leuteneg/www/BalancedSOFI/index.html> (accessed 10.03.15).
- [89] T.J. Gould, V.V. Verkhusha, S.T. Hess, *Nat. Protoc.* 4 (2009) 291–308, <http://dx.doi.org/10.1038/nprot.2008.246>.
- [90] piShaper – Versatile Beam Shaping Optics, (n.d.), [http://www.pishaper.com/shaper\\_6\\_6.php](http://www.pishaper.com/shaper_6_6.php) (accessed 10.03.15).
- [91] Focusing and Collimating, (n.d.), <http://www.newport.com/Focusing-and-Collimating/141191/1033/content.aspx> (accessed 4.03.15).
- [92] T. Holm, T. Klein, A. Löscherberger, T. Klamp, G. Wiebusch, S. Van De Linde, et al., *ChemPhysChem* 15 (2014) 651–654, <http://dx.doi.org/10.1002/cphc.201300739>.
- [93] How to use Engineered Diffusers, (n.d.). [http://www.rpcphotonics.com/how\\_to.asp](http://www.rpcphotonics.com/how_to.asp) (accessed 10.03.15).
- [94] J. Schindelin, I. Arganda-Carreras, E. Frise, V. Kaynig, M. Longair, T. Pietzsch, et al., *Nat. Methods* 9 (2012) 676–682, <http://dx.doi.org/10.1038/nmeth.2019>.